Collapse of the Kondo state and ferromagnetic quantum phase transition in YbFe_{2}Zn_{20}

Udhara S. Kaluarachchi, Li Xiang, Jianjun Ying, Tai Kong, Viktor Struzhkin, Alexander Gavriliuk, Sergey L. Bud'ko, and Paul C. Canfield

Collapse of Kondo state and ferromagnetic quantum phase transition in YbFe$_2$Zn$_{20}$

Udhara S. Kaluarachchi,[1, 2] Li Xiang,[1, 2] Jianjun Ying,[3, 4] Tai Kong,[1, 2] Viktor Struzhkin,[3] Alexander Gavriliuk,[5, 6, 7] Sergey L. Bud'ko,[1, 2] and Paul C. Canfield[1, 2]

[1] *Ames Laboratory, US Department of Energy, Iowa State University, Ames, Iowa 50011, USA*
[2] *Department of Physics and Astronomy, Iowa State University, Ames, Iowa 50011, U.S.A.*
[3] *Geophysical Laboratory, Carnegie Institution of Washington, Washington, DC 20015, USA*
[4] *HPCAT, Geophysical Laboratory, Carnegie Institution of Washington, Argonne, Illinois 60439, USA*
[5] *FSRC Crystallography and Photonics of Russian Academy of Sciences, Moscow 119333, Russia*
[6] *Institute for Nuclear Research, Russian Academy of Sciences, Moscow, Troitsk, 108840, Russia*
[7] *REC Functional Nanomaterials, Immanuel Kant Baltic Federal University, 236041 Kaliningrad, Russia*
(Dated: October 18, 2018)

We present the electrical resistivity data under application of pressures up to ∼ 26 GPa and down to 50 mK temperatures on YbFe$_2$Zn$_{20}$. We find a pressure induced magnetic phase transition with an onset at $p_c = 18.2 \pm 0.8$ GPa. At ambient pressure, YbFe$_2$Zn$_{20}$ manifests a heavy fermion, non-magnetic ground state and the Fermi liquid behavior at low temperatures. As pressure is increased, the power law exponent in resistivity, n, deviates significantly from Fermi liquid behavior and tends to saturate with $n = 1$ near p_c. A pronounced resistivity maximum, $T_{\max}$, which scales with Kondo temperature is observed. $T_{\max}$ decreases with increasing pressure and flattened out near p_c indicating the suppression of Kondo exchange interaction. For $p > p_c$, $T_{\max}$ shows a sudden upward shift, most likely becoming associated with crystal electric field scattering. Application of magnetic field for $p > p_c$ broadens the transition and shifts it toward the higher temperature, which is a typical behavior of a transition towards a ferromagnetic state, or a state with a significant ferromagnetic component. The magnetic transition appears to abruptly develop above p_c, suggesting probable first-order (with changing pressure) nature of the transition; once stabilized, the ordering temperature does not depend on pressure up to ∼ 26 GPa. Taken as a whole, these data suggest that YbFe$_2$Zn$_{20}$ has a quantum phase transition at $p_c = 18.2$ GPa associated with the avoided quantum criticality in metallic ferromagnets.

INTRODUCTION

Among the rare-earth-based intermetallic compounds, Ce and Yb -based materials have attracted much attention due to their peculiar properties [1–14]. The properties of these compounds are usually dominated by two characteristic energy scales: Ruderman-Kittel-Kasuya-Yosida (RKKY) [15–17] and Kondo [18, 19] interaction energies. The exchange interaction, J, which determines the interaction energy between local moments and conduction electron, $T_K \propto e^{-1/J}$, is also responsible for the coupling between local moments through the RKKY interaction, $T_{RKKY} \propto J^2$. Hence, the ground state of these compounds is determined by the competition between these two energy scales and often described by the Doniach phase diagram [20]. When $T_K \gg T_{RKKY}$ the ground state in nonmagnetic and when $T_K \ll T_{RKKY}$, magnetic order can be established. The most interesting situation occurs when the two energy scales are comparable and the system can be tuned through a $T = 0$ K magnetic instability at a quantum phase transition (QPT). By tuning the interaction via pressure, chemical substitution or magnetic field, the magnetic ordering temperature could be driven to $T = 0$ and quantum phase transition could happen. If the *second − order* magnetic phase transition is continuously suppressed to zero temperature, which is often seen in antiferromagnetic systems, then the term quantum critical point (QCP) is used[21–26]. If mag-

netic phase transition becomes of first order before being suppressed to zero temperature[27–30] the QPT term is used. In ferromagnetic metallic systems quantum criticality can be avoided either by the QPT or by the appearance of a modulated magnetic phase[31–33].

Often Yb is considered as a "hole" equivalent of Ce. In contrast to Ce compounds, where magnetic ordering is suppressed by pressure, in Yb systems, increasing pressure can tune the system from a nonmagnetic state to a magnetic one [8, 12]. There are only a few examples of the pressure induced, nonmagnetic-to-magnetic phase transitions in Yb compounds [2, 5, 6, 22, 34–38] and, so far, superconductivity has been reported in only two materials [11, 39].

The YbT_2Zn$_{20}$ (T = Fe, Ru, Os, Co, Rh, Ir) series is a Yb-based heavy fermion system [40–44] which belongs to the RT_2Zn$_{20}$ family [45]. For all six members, at high temperature, the magnetic susceptibility measurements show Curie-Weiss behavior with the effective moment close to the Yb^{3+} [40, 41]. In the resistivity measurements, there are no signs for the magnetic ordering down to 20 mK [40, 41]. Among this YbT_2Zn$_{20}$ series, YbCo$_2$Zn$_{20}$ has the lowest T_K and the largest Sommerfeld coefficient of the six members [40, 41]. By combining the Doniach model with this small T_K and large Sommerfeld coefficient, one can assume that YbCo$_2$Zn$_{20}$ is close to a possible magnetic QCP. With this idea, Saiga *et al.* [22] performed a high pressure resistivity measure-

ment on $YbCo_2Zn_{20}$ and observed a pressure induced QCP at a critical pressure $\sim 1\,\text{GPa}$ and antiferromagnetic (AFM) ordering at higher pressures. Apart from this, a field induced ordered phase has been observed at the ambient pressure in $YbCo_2Zn_{20}$, possibly due to the crystal electric field level crossing [46–51]. A pressure induced QCP has also been estimated for $YbIr_2Zn_{20}$ ($\approx 5.2\,\text{GPa}$) and $YbRh_2Zn_{20}$ ($\approx 5.2\,\text{GPa}$), however, for $YbRh_2Zn_{20}$ no pressure induced magnetic transitions have been observed so far [23–25, 52].

Several years ago, high pressure resistivity measurements were performed up to $8.23\,\text{GPa}$ for $YbFe_2Zn_{20}$ [53]. Increasing pressure drives T_K to lower values and enhanced the A-coefficient ($\Delta\rho(T) \propto AT^2$); a QCP of $\sim 10\,\text{GPa}$ was inferred [53]. In this work, by employing a diamond anvil cell in a dilution refrigerator, we extend the pressure range up to $\sim 26\,\text{GPa}$ and lower the base temperature to $50\,\text{mK}$. As a result we find a clear feature in resistivity that we identify as a magnetic phase transition in $YbFe_2Zn_{20}$ for $p > 18.2\,\text{GPa}$. The transition temperature is about $1\,\text{K}$ and does not change with further increase of pressures up to $26\,\text{GPa}$. We tentatively identify the transition as ferromagnetic in nature and associate the step-like feature in $T_C(p)$ with an avoided quantum criticality QPT.

EXPERIMENTAL METHODS

Single crystals used for this study were grown using a high-temperature solution growth technique [54, 55] with the help of frit-disc crucible set [56]. More details about the crystal growth can be found in Refs. 40, 57, and 58. Temperature and field dependent resistivity measurements were carried out using a Quantum Design Physical Property Measurement System from $1.8\,\text{K}$ to $300\,\text{K}$. A dilution refrigerator option was utilized to perform measurements down to $50\,\text{mK}$. The resistivity was measured using the van der Pauw method [59, 60] with ac-current ($I = 0.005\,\text{mA}$, $f = 18.3$ and $21.3\,\text{Hz}$) parallel to the [111] plane and a magnetic field was applied perpendicular to the current plane. A miniature diamond anvil cell [61], with $300\,\mu\text{m}$ culets, was used to generate the pressure for the resistivity measurement and KCl powder was used as a pressure transmitting medium. The temperature gradient between the dilution refrigerator thermometer and sensor positioned on miniature diamond anvil cell close to the anvils was evaluated in a separate experiment and was found negligible with the protocol of the measurement used in this work. Single crystals with a typical dimension of $80 \times 80 \times 20\,\mu\text{m}^3$ were loaded into the sample chamber with an inner diameter of $130\,\mu\text{m}$ made out of a cubic BN gasket. Pressure was applied at room temperature and ruby fluorescence, at $300\,\text{K}$ was used to determine the pressure[62].
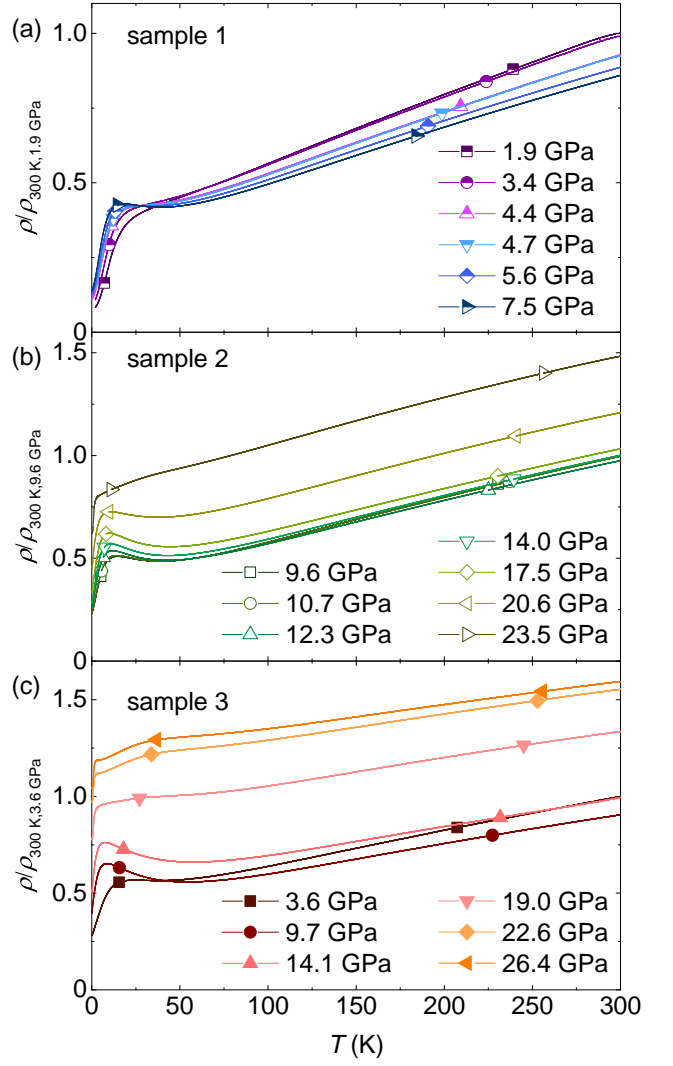

FIG. 1. (Color online) Temperature dependence of the normalized resistivity of three different samples of $YbFe_2Zn_{20}$: (a) sample 1, (b) sample 2 and (c) sample 3. Data have been normalized to the lowest pressure $300\,\text{K}$ resistivity value of each sample. Un-normalized curves are shown in appendix (Fig. A.1).

RESULTS AND DISCUSSION

Temperature dependent resistivity measurements on three different samples of $YbFe_2Zn_{20}$ under pressures up to $26.4\,\text{GPa}$ are shown in Fig. 1. For each pressure, resistivity values are normalized to the lowest pressure, $300\,\text{K}$ resistivity value of each sample. For sample 1, when increasing the pressure, the $300\,\text{K}$ resistivity, ρ_{300K}, is monotonically suppressed, which is similar to Ref. 53. For sample 2 and 3, as indicated in Figs. 1 (b) and (c), ρ_{300K} shows a non-monotonic dependence on pressure when higher pressure values are achieved. However, for $p \lesssim 18\,\text{GPa}$, ρ_{300K} shows relatively small variation with
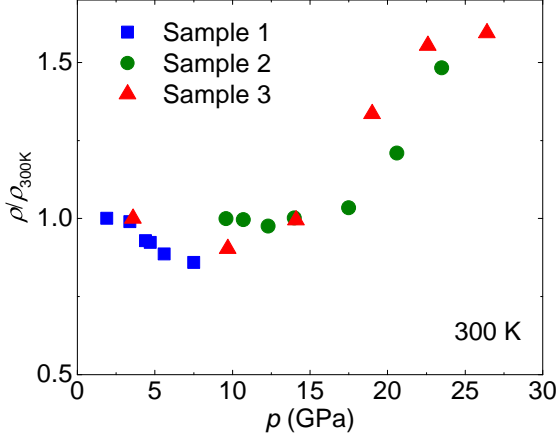
FIG. 2. (Color online) Pressure dependence of the normalized resistivity at 300 K. For each samples, ρ is normalized by the lowest pressure 300 K resistivity value of each sample. Unnormalized curves are shown in appendix (Fig. A.2 (c)).

pressure, while for $p \gtrsim 18$ GPa, ρ_{300K} systematically increases with pressure. Fig. 2 presents the pressure evolution of the normalized ρ_{300K} with pressure. As indicated in the figure, ρ_{300K} stays relatively flat for $p \lesssim 18$ GPa and continuously increases for $p \gtrsim 18$ GPa. Fig. 3 presents a low temperature expanded view of the data presented in Fig. 1. In addition to the increased ρ_{300K} for $p \gtrsim 18$ GPa there is also the clear onset of a relatively sharp, low temperature feature (Fig. 3) for $p \gtrsim 20$ GPa. Whereas these are qualitative changes we will now examine these data quantitatively.

For all measured pressures, for $T > 50$ K, the resistivity data show a nearly linear temperature dependence (Fig. 1). It is worth noting that the high-temperature slope (250 K $< T < 300$ K) of the resistivity decreases with increasing pressure up to about 10 GPa and then remains constant for higher pressures. Below 50 K, there is a broad shoulder in the resistivity data for $p < 3.4$ GPa that changes into a broad maximum ($T_{\max}$) with pressure increasing above 3.6 GPa. The value of $T_{\max}$ usually scales with the Kondo temperature, T_{K}[63–65]. It moves to lower temperatures with increasing pressure up to about 20 GPa and then shows a sudden increment for $p > 20$ GPa. The behavior of pressure dependence of the $T_{\max}$ (for $p < 9.6$ GPa) is consistent with the previous work [53].

The total resistivity of the $YbFe_2Zn_{20}$ can be expressed as a combination of normal metallic behavior and a magnetic contribution. As mentioned above, the high-temperature resistivity shows a nearly linear temperature dependence, indicating that phonon scattering is dominant in the high temperature range. Normal metallic behavior can be approximated by considering
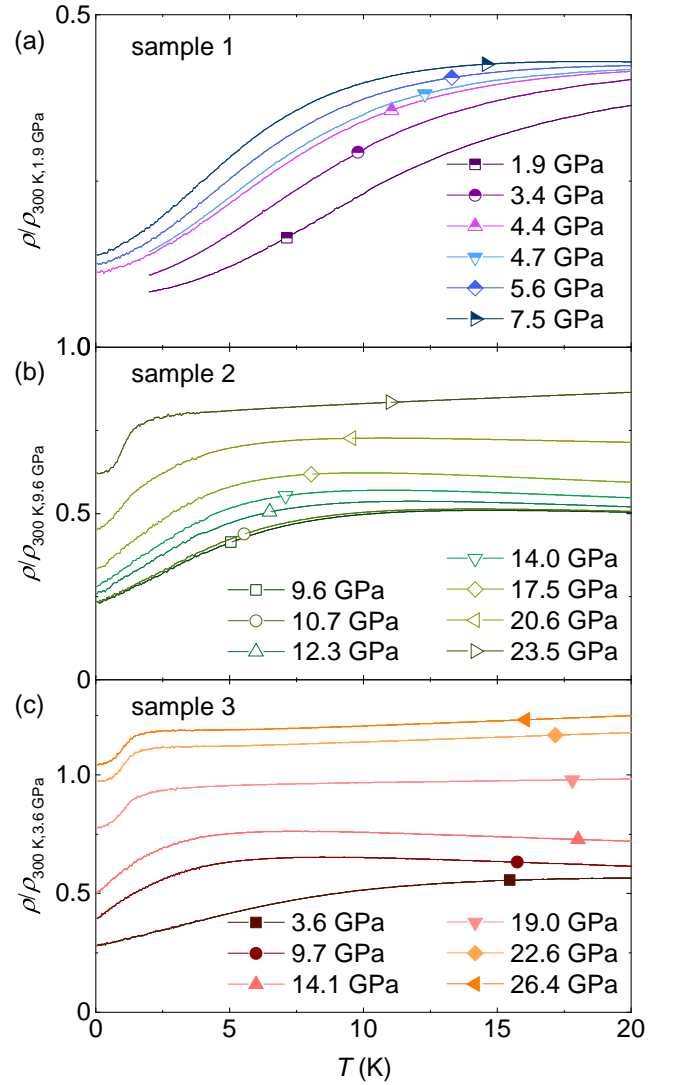

FIG. 3. (Color online) Blowup of the low temperature resistivity as in Fig. 1. Resistivity was measured down to 1.8 K for the first three pressures of sample 1, all the others have been measured down to 50 mK.

the temperature dependent resistivity of non-magnetic $LuFe_2Zn_{20}$. Therefore, the magnetic contribution to the resistivity of $YbFe_2Zn_{20}$ can be estimated by subtracting the $LuFe_2Zn_{20}$ resistivity data from $YbFe_2Zn_{20}$ data. Since the residual resistivity values of our samples show non-monotonic increments, first we have to subtract their residual resistivity values for each data set and then normalize the high temperature ($T > 275$ K) slope of the resistivity to that of $LuFe_2Zn_{20}$. This can be written as

$$\rho_{mag}(T) = (\rho_{\mathrm{Yb}} - \rho_{\mathrm{Yb,0}}) \frac{\frac{\mathrm{d}\rho_{\mathrm{Lu,R}}}{\mathrm{d}T}}{\frac{\mathrm{d}\rho_{\mathrm{Yb,R}}}{\mathrm{d}T}}\bigg|_{275K} - (\rho_{\mathrm{Lu}} - \rho_{\mathrm{Lu,0}}) \quad (1)$$

Similar analysis has been used to determine the $\rho_{mag}(T)$ in Ref. 43. $\rho_{mag}(T)$ data for samples 2 and 3 are shown in

Figs. 4 (a) and (b) respectively. For both samples, T_{max1} decreases with increasing pressure up to about 20 GPa and then shows a sudden change (jump up in temperature) for higher pressures. T_{max2} is the temperature corresponding to this higher pressure, broad, maximum in the $\rho_{mag}(T)$ low temperature data. The solid black triangles and open red squares indicate the T_{max1} and T_{max2} respectively.

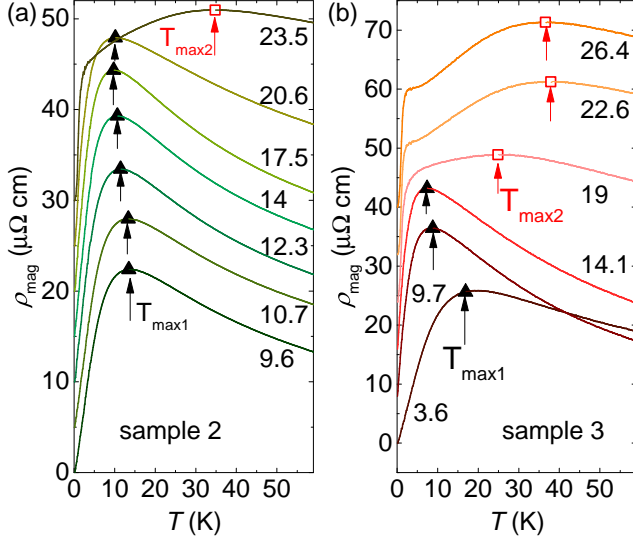FIG. 4. (Color online) Temperature dependent ρ_{mag} for (a) sample 2 and (b) sample 3. ρ_{mag} is obtained from Eq. 1 (see text below). The solid black triangles\arrows and open red squares\arrows indicate T_{max1} and T_{max2} respectively. Data are offset for clarity.

The evolution of the low temperature resistivity for samples 2 and 3 are shown in Figs. 5 (a) and (b) respectively. For $T < T_{max}$ and $p < 18.2$ GPa, the resistivity of both samples decreases with decreasing temperature and there is no pronounced anomaly down to 50 mK. When the pressure exceeds $p_c = 18.2 \pm 0.8$ GPa, the resistivity shows a kink/sharp drop, suggesting a loss of spin-disorder-scattering and magnetic ordering at T_M. The peak in the temperature derivative of the resistivity $d\rho/dT$ is used to determine the ordering temperature, T_M, as shown in Figs. 5 (c) and (d). As can be seen, the peak position does not change with the pressure and remains essentially the same up to 26 GPa. From the resistivity measurements, we cannot determine the nature of the magnetic transition, however, as shown in Fig. 6, application of magnetic field broadens the kink/sharp drop of the resistivity and moves it to higher temperatures, which suggests that this is not a structural phase transition. Instead, this is typical behavior for a transition towards a ferromagnetic state, or a state with a significant ferromagnetic component.

A pressure-temperature phase diagram can be constructed and shown in Fig. 7 using the data from Figs. 4
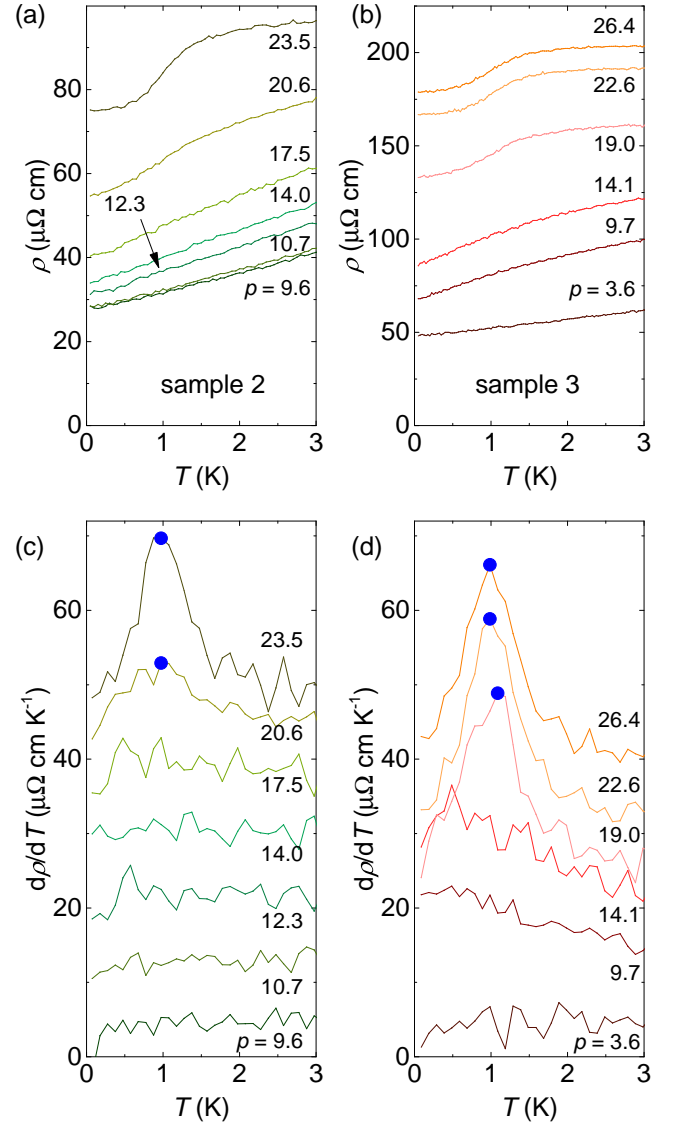

FIG. 5. (Color online) Low temperature resistivity of (a) sample 2 and (b) sample 3 and (c),(d) their corresponding temperature derivatives. Solid blue circles in (c) and (d) represent the criteria (peak of the $d\rho/dT$) used to obtain the transition temperature. Curves in (c) and (d) are offset by increments of $8\,\mu\Omega\,cm\,K^{-1}$ for clarity.

and 5 as well as data from Ref. 53. Black solid triangles and red open squares represent the data obtained from Fig. 4. The T_{max} obtained from Ref. 53 is represented by open green triangles.

Figs. 7 and 2 demonstrate three changes that take place as pressure increases through $p \sim 20$ GPa. At low temperatures (~ 1 K) there is the sudden appearance of a transition that is arguably ferromagnetic. At intermediate temperatures there is the disappearance of an ~ 10 K resistive maximum associated with the Kondo effect and the appearance of an 30-40 K resistive feature that is
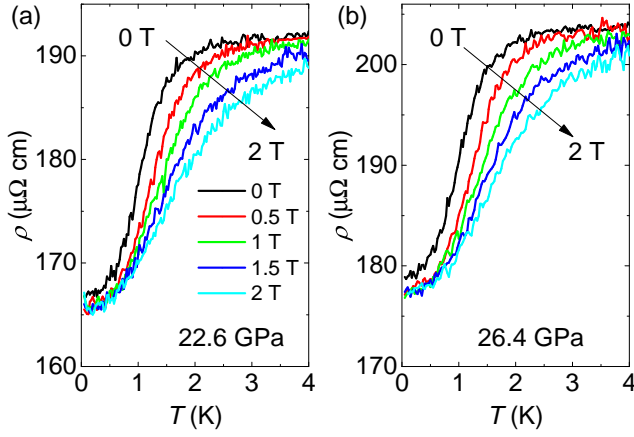
FIG. 6. (Color online) Temperature dependence of the resistivity at various magnetic fields for (a) $p = 22.6$ GPa and (b) $p = 26.4$ GPa.

most likely associated with CEF splitting [66, 67]. At higher temperatures, all the way up to room temperature, there is a marked increase in resistivity that starts around 15 GPa and appears to saturate by ~ 25 GPa. Taking these three observations together, our results strongly suggest that by ~ 20 GPa there is a band structure change associated with the droping of the Yb-$4f$-levels below the Fermi level. As a result, the Yb-$4f$-levels stop being hybridized and the system enters the magnetic regime in the Doniach phase diagram.

These results can be put in the context of the RFe$_2$Zn$_{20}$ (R = Gd-Tm) series which shows a clear de Gennes scaling of its ferromagnetic ordering temperature [43, 57]. According to the de Gennes scaling, if Yb^{3+} were to be purely local-moment-like, YbFe$_2$Zn$_{20}$ would order ferromagnetically at about 1 K. This is essentially what we find for $p > p_c$. The suggested pressure-induced ferromagnetic ordering in YbFe$_2$Zn$_{20}$ is not too surprising, if we look at other intermetallic compounds in RT_2Zn$_{20}$ family[41, 43]. Taking GdT_2Zn$_{20}$ series for example, ferromagnetic ordered ground state is found for members in the iron column (T = Fe, Ru and Os) while antiferromagnetic ordered ground state in the cobalt column (T = Co, Rh and Ir) [41]. Moreover, the pressure-induced ordered states in YbCo$_2$Zn$_{20}$ and YbIr$_2$Zn$_{20}$ have also been suggested as AFM ordering[25, 49]. Taking YbFe$_2$Zn$_{20}$ in this study together, RT_2Zn$_{20}$ family seems to follow the rule that for the iron column members, ferromagnetic ordering is expected, while for the cobalt column members, antiferromagnetic ordering is expected.

T_M appears to abruptly develop above p_c suggesting the first-order nature of the quantum phase transition at p_c. This is consistent with the growing number of examples of avoided quantum criticality in ferromagnetic metals[27, 32, 68, 69]. According to the current theoretical understanding, a continuous PM to FM tran-

sition is not possible at $T = 0$ K, when suppressing the FM phase with a clean parameter such as pressure [70]. Two possibilities have been proposed [71, 72]; either the transition becomes of the first order [27–30] or the modulated magnetic phase appears to replace the ferromagnetic one [31–33]. In order to check for hysteresis effects (first order transition), the resistivity measurements were carried out with both increasing and decreasing temperatures at 26.4 GPa (see Fig. 8). However, no hysteretic behavior is observed. This could be due to a weak-first-order transition, where the hysteresis is small and may not be detected experimentally. Also, it could be due to 26.4 GPa being higher than the pressure that corresponds to the tricritical point, so that, at 26.4 GPa, the transition is second order in temperature[27, 29, 32, 73–75].
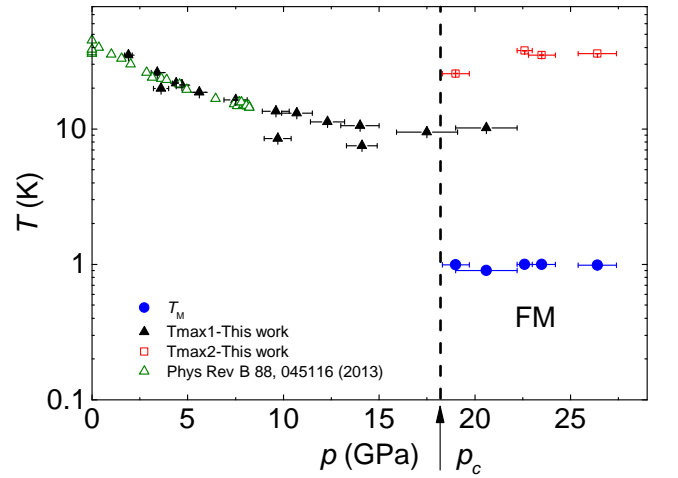

FIG. 7. (Color online) Temperature-pressure phase diagram of YbFe$_2$Zn$_{20}$ as determined from resistivity measurement. T_M, T_{max1} and T_{max2} are obtained using the criteria described in Fig. 4 and 5. The green open triangles are obtained from Ref. 53. Vertical arrow represents the critical pressure $p_c = 18.2 \pm 0.8$ GPa for ferromagnetic transition as well as 4f-localization. The error bars of p are determined by performing ruby fluorescence on several locations inside the sample space. The error bars of temperature are determined as half the data spacing.

Let's consider more details about the temperature variation of the resistivity. Figs 9 (a)-(c) show the ρ-ρ_0 versus T for sample 1, 2 and 3 to emphasize the low-temperature exponent, n, which appears as the slope on a log-log scale. At low-pressures (in Fig. 9 (a) $p < 3.4$ GPa), ρ-ρ_0 obeys T^2 and for the intermediate pressures ($p \sim 6$ GPa) it follows $T^{1.5}$. For higher pressures (9 GPa $< p < 18$ GPa), ρ-ρ_0 shows linear T dependence over a wide range of temperature. A T-linear resistance has been observed in several compounds, such as; CeCoIn$_5$ [76], CeRhIn$_5$ [77, 78], YbRh$_2$Si$_2$ [21, 79, 80], YbAgGe[9, 81] and CeNi$_2$Ge$_2$ [82]. Evolution of the temperature power-law exponent n with pressure is summarized in Fig. 9 (d). The value of n is ob-

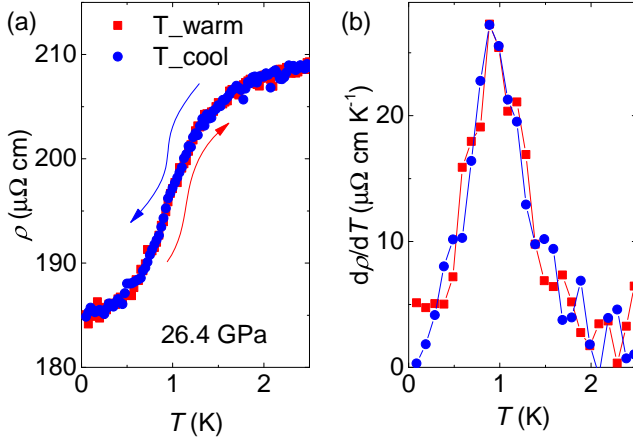FIG. 8. (Color online) (a) Temperature dependence of the resistivity at $26.4\,\mathrm{GPa}$ for increasing (red solid squares) and decreasing (blue solid circles) temperature. (b) Temperature derivative of ρ for both increasing (red solid squares) and decreasing (blue solid circles) temperature.

tained from a sliding window fit to $\rho\text{-}\rho_0 = A\,T^n$, where ρ_0 is obtained from the fit at the lowest temperature. Since the data have been taken down to $0.05\,\mathrm{K}$, the value of ρ_0 can be obtained more accurately than was possible for Ref. 53. As can be seen, n is clearly deviating from 2 for higher pressures. Power-law analysis from Ref. 53 indicates $n = 2$ even at $p \sim 8\,\mathrm{GPa}$ (see Figs. 5 and 9 in Ref. 53). This most likely led to the low estimated value of p_c based on the divergence of A-coefficient in Ref. 53. For $p > p_c$ the low temperature loss of spin disorder feature has $\propto T^n$ behavior most likely associated with spin excitation scattering not too far below T_c. As indicated in Fig. 9 (d), as pressure is increased above p_c, n quickly deviates from 1.

From the constructed $p - T$ phase diagram (Fig. 7), it is shown that for YbFe$_2$Zn$_{20}$, at the low temperature region, the associated Kondo temperature $T_{\mathrm{max}1}$ is first suppressed with increasing pressure. At p_c, a possibly ferromagnetic transition T_M suddenly appears at $\sim$ 1 K and stays unchanged with further increasing pressure. This suggests that for YbFe$_2$Zn$_{20}$, the quantum criticality is avoided by going through a first-order QPT under pressure, which is in contrast to the YbCo$_2$Zn$_{20}$ and YbIr$_2$Zn$_{20}$, where they enter AFM ordered states through QCP[22, 25, 49]. At high temperature, a continuously increase of the resistivity with pressure was observed for $p \gtrsim p_c$ (Fig. 2), suggesting that the suppressing of hybridization and developing of the Yb^{3+} local moment is more continuous in nature.
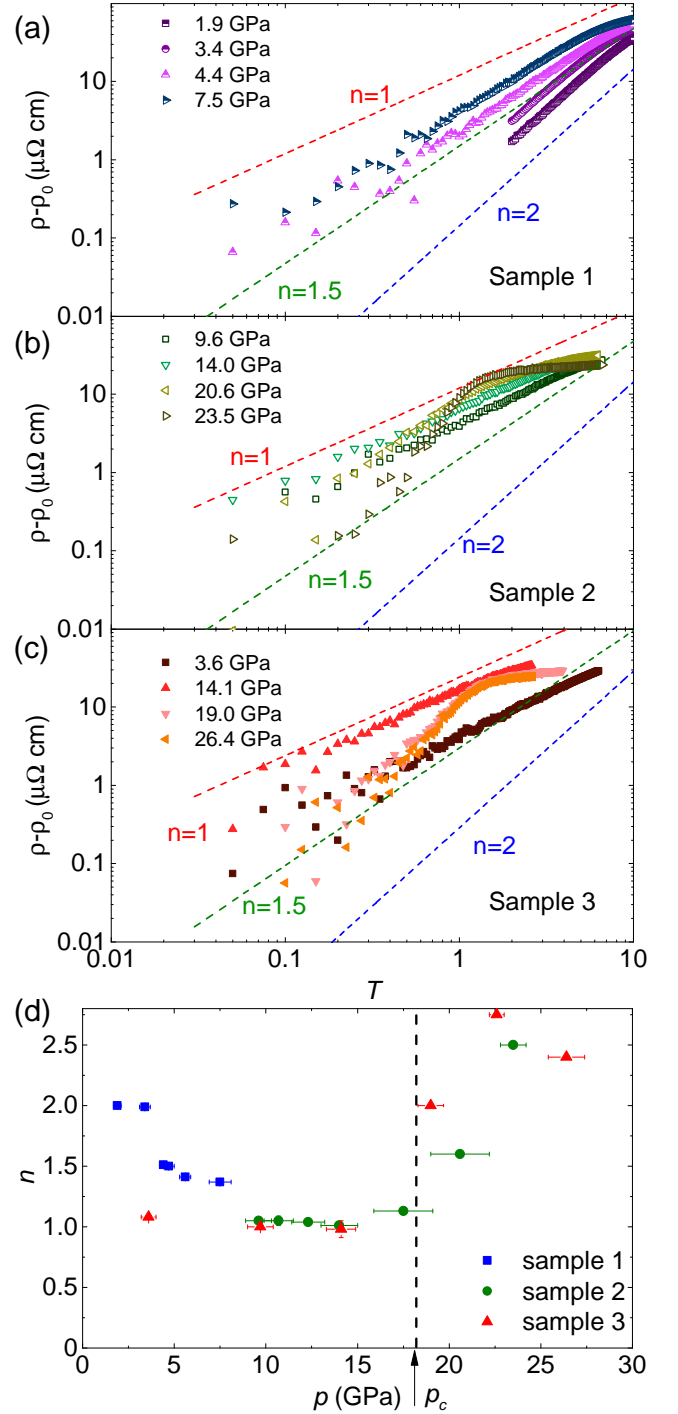

FIG. 9. (Color online) $\rho\text{-}\rho_0$ vs T for (a) sample 1 (b) sample 2 and (c) sample 3 in log-log scale for selected pressures. The Red, green and blue dashed lines are guides showing slopes for various low-temperature exponents, $n = 1$, 1.5 and 2 respectively. (d) Evolution of n as a function of pressure. Corresponding n is obtained by fitting (a)-(c) with $\rho\text{-}\rho_0 = AT^n$. For $p > p_c$, fitting was done for $T < T_M$. Vertical arrow represents the critical pressure p_c.

CONCLUSIONS

In summary, we have measured the resistivity of $YbFe_2Zn_{20}$ up to $\sim 26\,GPa$ and down to $50\,mK$. Above a critical pressure, $p_c = 18.2 \pm 0.8\,GPa$, we observed the resistivity anomaly at $T_M \sim 1\,K$, which remains constant with increasing pressure. This anomaly appears to correspond to a transition towards a ferromagnetic state, or a state with a significant ferromagnetic component, since the application of magnetic field broadened the transition and moved it to higher temperature. Increasing pressure drives the T_{max}, the associated Kondo temperature, to lower values and flattening at pressures up to p_c indicating a decrease of the hybridization strength. Above p_c, T_{max} abruptly increases with pressure. In this pressure range T_{max} can be attributed to the crystal electric field effects. In heavy fermion non-magnetic phase, the low temperature power law exponent is deviated from the Fermi liquid behavior for $p > 3.4\,GPa$ and reached $n = 1$ for $9\,GPa < p < p_c$. The reason for this unusual exponent value, $n = 1$, over large range of pressure is not clear so far. Additionally, our data suggests that at $\sim p_c$ there is a band structure change associated with the dropping of 4f-levels below the Fermi level.
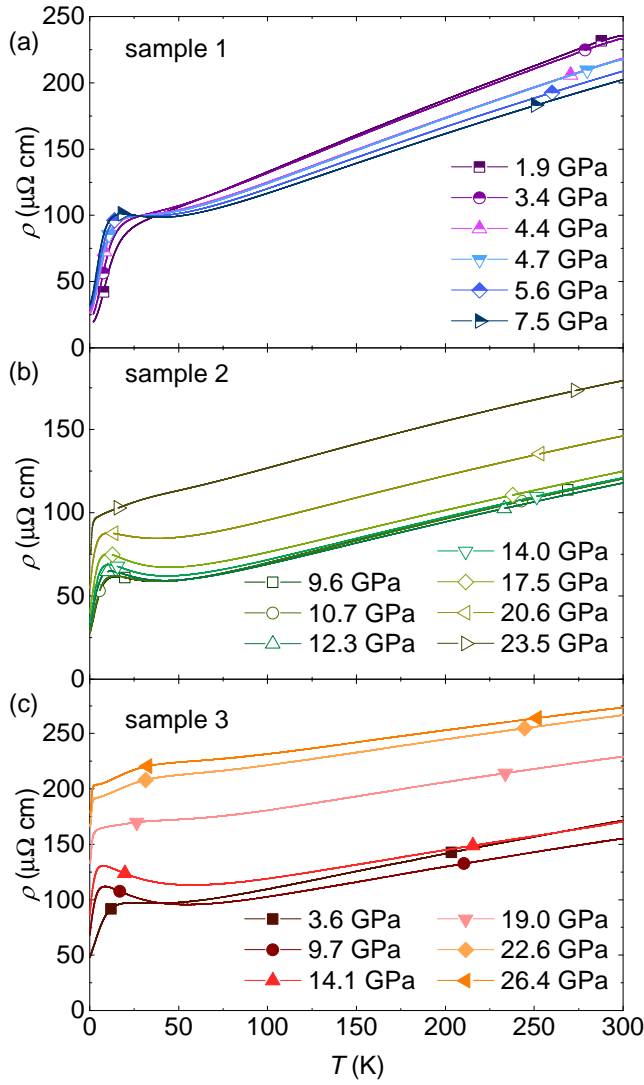
FIG. A.1. (Color online) Temperature dependence of the resistivity of three different samples of YbFe$_2$Zn$_{20}$: (a) sample 1, (b) sample 2 and (c) sample 3.
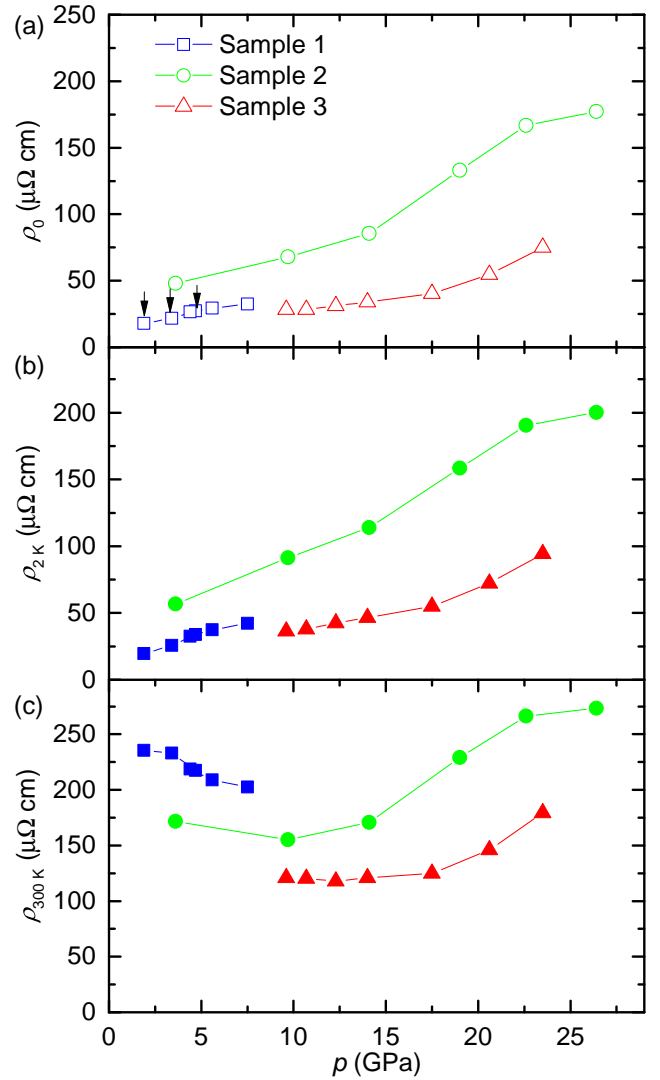
FIG. A.2. (Color online) Pressure dependence of resistivity ρ at different fixed timperatures. (a) ρ_0 values were obtained by extrapolating low temperature $\rho(T)$ data to 0 K. For sample 1, the first three pressures, measurements were done down to 2 K (arrows in (a)), for the rest, measurements were done down to 0.05 K. (b)Resistivity ρ at 2 K. (c)Resistivity ρ at 300 K.

APPENDIX

Fig. A.1 presents the temperature dependence of the resistivity of three different samples without normalization. Fig. A.2 presents the pressure dependence of the resistivity values at different fixed temperatures. (a) Extrapolated 0 K resistivity values ρ_0 by fitting low temperature $\rho(T)$ data, (b) ρ at 2 K, (c) ρ at 300 K. Fig. 2 is the normalized version of Fig. A.2 (c) obtained by dividing the 300 K resistivity value at the lowest pressure for each sample.

[1] R. Movshovich, A. Lacerda, P. C. Canfield, J. D. Thompson, and Z. Fisk, Phys. Rev. Lett. **73**, 492 (1994).
[2] A. L. Cornelius, J. S. Schilling, D. Mandrus, and J. D. Thompson, Phys. Rev. B **52**, R15699 (1995).
[3] F. Grosche, S. Julian, N. Mathur, and G. Lonzarich, Physica B **223**, 50 (1996).
[4] N. D. Mathur, F. M. Grosche, S. R. Julian, I. R. Walker, D. M. Freye, R. K. W. Haselwimmer, and G. G. Lonzarich, Nature **394**, 39 (1998).
[5] K. Alami-Yadri, H. Wilhelm, and D. Jaccard, Eur. Phys. J. B **6**, 5 (1998).

[6] H. Winkelmann, M. M. Abd-Elmeguid, H. Micklitz, J. P. Sanchez, P. Vulliet, K. Alami-Yadri, and D. Jaccard, Phys. Rev. B **60**, 3324 (1999).

[7] G. Knebel, D. Braithwaite, P. C. Canfield, G. Lapertot, and J. Flouquet, Phys. Rev. B **65**, 024425 (2001).

[8] G. R. Stewart, Rev. Mod. Phys. **73**, 797 (2001).

[9] S. L. Bud'ko, E. Morosan, and P. C. Canfield, Phys. Rev. B **69**, 014415 (2004).

[10] P. Coleman, "Heavy Fermions: Electrons at the Edge of Magnetism," in *Handbook of Magnetism and Advanced Magnetic Materials* (John Wiley & Sons, Ltd, 2007).

[11] S. Nakatsuji, K. Kuga, Y. Machida, T. Tayama, T. Sakakibara, Y. Karaki, H. Ishimoto, S. Yonezawa, Y. Maeno, E. Pearson, G. G. Lonzarich, L. Balicas, H. Lee, and Z. Fisk, Nature Physics **4**, 603 (2008).

[12] J. Flouquet and H. Harima, Kotai Bursuri **47** (2012).

[13] Q. Si and F. Steglich, Science **329**, 1161 (2010).

[14] A. Steppke, R. Kuchler, S. Lausberg, E. Lengyel, L. Steinke, R. Borth, T. Luhmann, C. Krellner, M. Nicklas, C. Geibel, F. Steglich, and M. Brando, Science **339**, 933 (2013).

[15] M. A. Ruderman and C. Kittel, Phys. Rev. **96**, 99 (1954).

[16] T. Kasuya, Progress of Theoretical Physics **16**, 45 (1956).

[17] K. Yosida, Phys. Rev. **106**, 893 (1957).

[18] J. Kondo, Progress of Theoretical Physics **32**, 37 (1964).

[19] A. C. Hewson, *The Kondo Problem to Heavy Fermions*, Cambridge Studies in Magnetism (Cambridge University Press, 1993).

[20] S. Doniach, Physica B & C **91**, 231 (1977).

[21] O. Trovarelli, C. Geibel, S. Mederle, C. Langhammer, F. M. Grosche, P. Gegenwart, M. Lang, G. Sparn, and F. Steglich, Phys. Rev. Lett. **85**, 626 (2000).

[22] Y. Saiga, K. Matsubayashi, T. Fujiwara, M. Kosaka, S. Katano, M. Hedo, T. Matsumoto, and Y. Uwatoko, J. Phys. Soc. Jpn. **77**, 053710 (2008).

[23] K. Matsubayashi, Y. Saiga, T. Matsumoto, and Y. Uwatoko, J. Phys. Conf. Ser. **150**, 042117 (2009).

[24] F. Honda, S. Yasui, S. Yoshiuchi, T. Takeuchi, R. Settai, and Y. Ōnuki, J. Phys. Soc. Jpn. **79**, 083709 (2010).

[25] F. Honda, Y. Taga, S. Yasui, S. Yoshiuchi, Y. Hirose, T. Takeuchi, R. Settai, and Y. Ōnuki, J. Phys. Soc. Jpn. **81**, SB063 (2012).

[26] E. D. Mun, S. L. Bud'ko, C. Martin, H. Kim, M. A. Tanatar, J.-H. Park, T. Murphy, G. M. Schmiedeshoff, N. Dilley, R. Prozorov, and P. C. Canfield, Phys. Rev. B **87**, 075120 (2013).

[27] V. Taufour, D. Aoki, G. Knebel, and J. Flouquet, Phys. Rev. Lett. **105**, 217201 (2010).

[28] N. Kabeya, H. Maekawa, K. Deguchi, N. Kimura, H. Aoki, and N. K. Sato, J. Phys. Soc. Jpn. **81**, 073706 (2012).

[29] V. Taufour, U. S. Kaluarachchi, R. Khasanov, M. C. Nguyen, Z. Guguchia, P. K. Biswas, P. Bonfà, R. De Renzi, X. Lin, S. K. Kim, E. D. Mun, H. Kim, Y. Furukawa, C.-Z. Wang, K.-M. Ho, S. L. Bud'ko, and P. C. Canfield, Phys. Rev. Lett. **117**, 037207 (2016).

[30] U. S. Kaluarachchi, V. Taufour, S. L. Bud'ko, and P. C. Canfield, Phys. Rev. B **97**, 045139 (2018).

[31] H. Kotegawa, T. Toyama, S. Kitagawa, H. Tou, R. Yamauchi, E. Matsuoka, and H. Sugawara, J. Phys. Soc. Jpn. **82**, 123711 (2013).

[32] U. S. Kaluarachchi, S. L. Bud'ko, P. C. Canfield, and V. Taufour, Nat. Commun. **8**, 546 (2017).

[33] S. Friedemann, W. J. Duncan, M. Hirschberger, T. W. Bauer, R. Kuchler, A. Neubauer, M. Brando, C. Pfleiderer, and F. M. Grosche, Nat. Phys. **14**, 62 (2017).

[34] H. Winkelmann, M. M. Abd-Elmeguid, H. Micklitz, J. P. Sanchez, C. Geibel, and F. Steglich, Phys. Rev. Lett. **81**, 4947 (1998).

[35] T. Nakano, M. Hedo, Y. Uwatoko, and E. Sampathkumaran, Solid State Commun **132**, 325 (2004).

[36] M. Schöppner, J. Moser, A. Kratzer, U. Potzel, J. M. Mignot, and G. M. Kalvius, Z. Phys. B **63**, 25 (1986).

[37] G. Knebel, D. Braithwaite, G. Lapertot, P. C. Canfield, and J. Flouquet, J. Phys. Condens. Matter **13**, 10935 (2001).

[38] H. Q. Yuan, M. Nicklas, Z. Hossain, C. Geibel, and F. Steglich, Phys. Rev. B **74**, 212403 (2006).

[39] E. Schuberth, M. Tippmann, L. Steinke, S. Lausberg, A. Steppke, M. Brando, C. Krellner, C. Geibel, R. Yu, Q. Si, and F. Steglich, Science **351**, 485 (2016).

[40] M. S. Torikachvili, S. Jia, E. D. Mun, S. T. Hannahs, R. C. Black, W. K. Neils, D. Martien, S. L. Bud'ko, and P. C. Canfield, Proc. Natl. Acad. Sci. **104**, 9960 (2007).

[41] S. Jia, N. Ni, G. D. Samolyuk, A. Safa-Sefat, K. Dennis, H. Ko, G. J. Miller, S. L. Bud'ko, and P. C. Canfield, Phys. Rev. B **77**, 104408 (2008).

[42] P. C. Canfield, S. Jia, E. D. Mun, S. L. Bud'ko, G. D. Samolyuk, and M. S. Torikachvili, Physica B **403**, 844 (2008).

[43] S. Jia, N. Ni, S. L. Bud'ko, and P. C. Canfield, Phys. Rev. B **80**, 104403 (2009).

[44] E. D. Mun, S. Jia, S. L. Bud'ko, and P. C. Canfield, Phys. Rev. B **86**, 115110 (2012).

[45] T. Nasch, W. Jeitschko, and U. C. Rodewald, Z. Naturforsch. B Chem. Sci. **52**, 1023 (1997).

[46] Y. Shimura, T. Sakakibara, S. Yoshiuchi, F. Honda, R. Settai, and Y. Ōnuki, J. Phys. Soc. Jpn. **80**, 073707 (2011).

[47] T. Takeuchi, M. Ohya, S. Yoshiuchi, M. Matsushita, F. Honda, R. Settai, and Y. Ōnuki, J. Phys. Conf. Ser. **273**, 012059 (2011).

[48] Y. Shimura, T. Sakakibara, S. Yoshiuchi, F. Honda, R. Settai, and Y. Ōnuki, J. Phys. Conf. Ser. **391**, 012066 (2012).

[49] Y. Taga, S. Yoshiuchi, M. Ohya, J. Sakaguchi, Y. Hirose, F. Honda, T. Takeuchi, R. Settai, and Y. Ōnuki, J. Phys. Soc. Jpn. **81**, SB064 (2012).

[50] T. Takeuchi, S. Yoshiuchi, M. Ohya, Y. Taga, Y. Hirose, K. Sugiyama, F. Honda, M. Hagiwara, K. Kindo, R. Settai, and Y. Ōnuki, J. Phys. Soc. Jpn. **80**, 114703 (2011).

[51] F. Honda, Y. Taga, Y. Hirose, S. Yoshiuchi, Y. Tomooka, M. Ohya, J. Sakaguchi, T. Takeuchi, R. Settai, Y. Shimura, T. Sakakibara, I. Sheikin, T. Tanaka, Y. Kubo, and Y. Ōnuki, J. Phys. Soc. Jpn. **83**, 044703 (2014).

[52] F. Honda, T. Takeuchi, S. Yasui, Y. Taga, S. Yoshiuchi, Y. Hirose, Y. Tomooka, K. Sugiyama, M. Hagiwara, K. Kindo, R. Settai, and Y. Ōnuki, J. Phys. Soc. Jpn. **82**, 084705 (2013).

[53] S. K. Kim, M. S. Torikachvili, S. L. Bud'ko, and P. C. Canfield, Phys. Rev. B **88**, 045116 (2013).

[54] P. C. Canfield and Z. Fisk, Philos. Mag. B **65**, 1117 (1992).

[55] P. C. Canfield and I. R. Fisher, J. Cryst. Growth **225**, 155 (2001).

[56] P. C. Canfield, T. Kong, U. S. Kaluarachchi, and N. H. Jo, Philos. Mag. **96**, 84 (2016).

[57] S. Jia, S. L. Bud'ko, G. D. Samolyuk, and P. C. Canfield, Nature Physics **3**, 334 (2007).

[58] T. Kong, V. Taufour, S. L. Bud'ko, and P. C. Canfield, Phys. Rev. B **95**, 155103 (2017).

[59] L. J. van der Pauw, Philips Research Reports **20**, 220 (1958).

[60] A. A. Ramadan, R. D. Gould, and A. Ashour, Thin Solid Films **239**, 272 (1994).

[61] A. G. Gavriliuk, A. A. Mironovich, and V. V. Struzhkin, Rev. Sci. Instrum. **80**, 043906 (2009).

[62] G. J. Piermarini, S. Block, J. D. Barnett, and R. A. Forman, J. Appl. Phys. **46**, 2774 (1975).

[63] A. Yoshimori and H. Kasai, Journal of Magnetism and Magnetic Materials **31-34**, 475 (1983).

[64] P. Coleman, Journal of Magnetism and Magnetic Materials **63-64**, 245 (1987).

[65] E. Bauer, R. Hauser, E. Gratz, K. Payer, G. Oomi, and T. Kagayama, Phys. Rev. B **48**, 15873 (1993).

[66] B. Cornut and B. Coqblin, Phys. Rev. B **5**, 4541 (1972).

[67] K. Hanzawa, K. Yamada, and K. Yosida, J. Magn. Magn. Mater **47**, 357 (1985).

[68] H. Kotegawa, V. Taufour, D. Aoki, G. Knebel, and J. Flouquet, J. Phys. Soc. Jpn. **80**, 083703 (2011).

[69] W. Kittler, V. Fritsch, F. Weber, G. Fischer, D. Lamago, G. André, and H. v. Löhneysen, Phys. Rev. B **88**, 165123 (2013).

[70] M. Brando, D. Belitz, F. M. Grosche, and T. R. Kirkpatrick, Rev. Mod. Phys. **88**, 025006 (2016).

[71] D. Belitz, T. R. Kirkpatrick, and T. Vojta, Phys. Rev. B **55**, 9452 (1997).

[72] D. Belitz, T. R. Kirkpatrick, and T. Vojta, Phys. Rev. Lett. **82**, 4707 (1999).

[73] D. Belitz, T. R. Kirkpatrick, and J. Rollbühler, Phys. Rev. Lett. **94**, 247205 (2005).

[74] Y. J. Uemura, T. Goko, I. M. Gat-Malureanu, J. P. Carlo, P. L. Russo, A. T. Savici, A. Aczel, G. J. MacDougall, J. A. Rodriguez, G. M. Luke, S. R. Dunsiger, A. McCollam, J. Arai, C. Pfleiderer, P. Boni, K. Yoshimura, E. Baggio-Saitovitch, M. B. Fontes, J. Larrea, Y. V. Sushko, and J. Sereni, Nat. Phys. **3**, 29 (2007).

[75] F. Lévy, I. Sheikin, and A. Huxley, Nat. Phys. **3**, 460 (2007).

[76] V. A. Sidorov, M. Nicklas, P. G. Pagliuso, J. L. Sarrao, Y. Bang, A. V. Balatsky, and J. D. Thompson, Phys. Rev. Lett. **89**, 157004 (2002).

[77] G. Knebel, D. Aoki, J.-P. Brison, and J. Flouquet, J. Phys. Soc. Jpn. **77**, 114704 (2008).

[78] T. Park, V. A. Sidorov, F. Ronning, J.-X. Zhu, Y. Tokiwa, H. Lee, E. D. Bauer, R. Movshovich, J. L. Sarrao, and J. D. Thompson, Nature **456**, 366 (2008).

[79] P. Gegenwart, J. Custers, C. Geibel, K. Neumaier, T. Tayama, K. Tenya, O. Trovarelli, and F. Steglich, Phys. Rev. Lett. **89**, 056402 (2002).

[80] J. Custers, P. Gegenwart, C. Geibel, F. Steglich, P. Coleman, and S. Paschen, Phys. Rev. Lett. **104**, 186402 (2010).

[81] P. G. Niklowitz, G. Knebel, J. Flouquet, S. L. Bud'ko, and P. C. Canfield, Phys. Rev. B **73**, 125101 (2006).

[82] F. M. Grosche, P. Agarwal, S. R. Julian, N. J. Wilson, R. K. W. Haselwimmer, S. J. S. Lister, N. D. Mathur, F. V. Carter, S. S. Saxena, and G. G. Lonzarich, J. Phys. Condens. Matter **12**, L533 (2000).